Nanoscale

PAPER

View Article Online
View Journal | View Issue

Cite this: *Nanoscale*, 2018, **10**, 10999

Three-dimensional sp^2 carbon networks prepared by ultrahigh temperature treatment for ultrafast lithium–sulfur batteries†

Chunping Ruan,[a] Zhi Yang,*[a] Huagui Nie,*[a] Xuemei Zhou,[b] Zeqing Guo,[a] Lu Wang,[a] Xingwei Ding,[a] Xi'an Chen[a] and Shaoming Huang*[a,b]

Received 12th April 2018,
Accepted 8th May 2018

DOI: 10.1039/c8nr02983k

rsc.li/nanoscale

The current challenge in the development of high-performance lithium–sulfur (Li–S) batteries is to facilitate the redox kinetics of sulfur species as well as to suppress the shuttle effect of polysulfides, especially at high current rates. Herein, aiming the application of Li–S at high current rates, we coupled a sp^2 carbon configuration consisting of 3D carbon nanotubes/graphene prepared by ultrahigh temperature treatment (2850 °C) with S (2850CNTs–Gra–S) for application in Li–S batteries. The 2850CNTs–Gra as the host material exhibits a nearly perfect sp^2 hybridized structure because ultrahigh temperature treatment not only repairs the raw defects in CNTs and graphene, but it also forms new sp^2 C–C bonds between them. The 3D sp^2 carbon network ensures ultrafast ion/electron transfer and efficient heat dissipation to protect the integrity of the separator when the Li–S battery is running at an ultrahigh rate. Based on these unique advantages, the 2850CNTs–Gra–S cathode shows a high current rate performance. Critically, it still delivers a considerable specific capacity after 1500 cycles even at a current rate of 15C and exhibits an extremely low capacity degradation rate of 0.0087% per cycle.

Rechargeable batteries with high energy density and long-term cycling stability are urgently needed for energy storage systems.[1,2] Lithium–sulfur batteries are regarded as one of the most promising candidates because of their high theoretical capacity (1675 mA h g^{-1}) and the natural abundance of sulfur.[3,4] However, there are three practical issues with the sulfur cathodes: (1) the shuttle effect of soluble polysulfide (PS) intermediates, (2) the poor electrical conductivity of sulfur, and (3) the volume variation of the cathode during cycling, which often leads to sluggish electrode kinetics and poor active material utilization.[5–8]

To overcome the abovementioned problems, a lot of strategies have been adopted, such as immobilizing sulfur in conductive carbon materials,[9–18] introduction of polar inorganic materials (Al_2O_3,[19,20] TiO_2,[21] WS_2,[22] and VN[23]) to the cathode, and incorporating PS-scission reagents in the interlayer.[27] The aforementioned methods improve the capacity and cycling stability of Li–S batteries to some degree. However, to meet the practical requirements of electric vehicles or large-scale energy storage systems, the batteries usually need to withstand thousands of charge–discharge cycles, especially at high current rates. There have been only a few studies of the electrochemical properties of Li–S batteries at ultrahigh current rates, especially above 10C.[24,25] This is mainly due to the following points: (1) the introduced materials (*e.g.*, TiO_2 [26] and dithiothreitol (DTT))[27] always have poor conductivity or are even insulating, which will greatly increase the polarization voltage of the battery, particularly at high rates. (2) The fast conversion reaction corresponds to fast accumulation of Li_2S/S at high current density, causing large volume changes, thus the host material should be as resilient as possible. (3) A higher current density could cause increased internal joule heating to the cathode, which affects the integrity of the separator and influences the safety of lithium. Considering the critical issues described above, developing a new structure that can achieve ultrafast ion/electron transfer, accommodate the volume changes of the electrode, and possess excellent heat dissipation functionality is highly desirable to achieve high-power long-life Li–S batteries.

Carbon materials with an ideal sp^2 hybridized structure and high graphitization degree have many intriguing properties, including excellent electrical and thermal conductivity,

[a]*Nanomaterials & Chemistry Key Laboratory, Wenzhou University, Wenzhou, 325027, China. E-mail: yang201079@126.com, huaguinie@126.com, smhuang@wzu.edu.cn*
[b]*School of Material and Energy, Guangdong University of Technology, Guangzhou, 510006, China*

†Electronic supplementary information (ESI) available: The additional SEM, TEM, XPS, TGA and electrochemical performance. See DOI: 10.1039/c8nr02983k

high chemical stability, and excellent mechanical performance. It has also been confirmed that heat treatment at ultrahigh temperature (>2400 °C) can greatly improve the graphitization degree of graphene, resulting in high electrical and thermal conductivity, and excellent flexibility performance.[28,29] These factors motivated us to determine what would happen when sp^2 hybridized carbon networks are treated at ultrahigh temperature and then introduced into the Li–S system. Research on the application of ideal sp^2 carbon materials in the Li–S system has been rare.

In this study, we prepared a Li–S battery configuration by coupling a sp^2 carbon network consisting of 3D carbon nanotubes/graphene prepared by ultrahigh temperature treatment (2850 °C) with S (2850CNTs–Gra–S). The 2850CNTs–Gra as the host material exhibits a nearly perfect sp^2 hybridized structure because ultrahigh temperature treatment not only repairs the raw defects in single CNTs and graphene, but it also forms new sp^2 C–C bonds between them. The 3D network ensures ultrafast ion/electron transfer and efficient heat dissipation to protect the integrity of the separator when the Li–S battery is running at an ultrahigh rate. Based on these unique advantages, the 2850CNTs–Gra–S cathode shows high current rate performance. Critically, it still delivers a considerable specific capacity after 1500 cycles even at a current rate of 15C and exhibits an extremely low capacity degradation rate of 0.0087% per cycle. Such a low capacity decay rate of 0.0087% (>10C) has rarely been reported.

Results and discussion

In this work, the 3D sp^2 hybridized carbon network with an ultrahigh graphitization degree acts as a host material for sulfur fixation. Typically, commercial CNTs and graphene were ultrasonically dispersed to form a 3D network structure, and then the uniform mixture was heated at 2850 °C for 2 h in an ultrahigh temperature furnace. The obtained host material is defined as 2850CNTs–Gra. For comparison, other carbon samples were also obtained under different conditions, such as different temperatures, annealing times and mass ratios of the carbon materials, and their physical parameters are listed in Table S1.† The resulting materials are called CNTs–Gra, 2250CNTs–Gra, 2550CNTs–Gra, 2850CNTs–Gra, 2850^4CNTs–Gra, 2850CNTs, 2850Gra, and so forth. 2850CNTs–Gra was selected as the optimal host material for subsequent Li–S battery experiments after comparing the rate performance test results (Fig. S1†).

The scanning electron microscopy (SEM) and transmission electron microscopy (TEM) images of 2850CNTs–Gra are shown in Fig. 1a and Fig. S2a,† respectively. A 3D network structure of CNTs intercalated in graphene can be clearly observed. Notably, compared with the Raman spectrum of CNTs–Gra, in the Raman spectrum of 2850CNTs–Gra, the peak of the D band at about 1350 cm^{-2} disappears and a new peak of the 2D band (caused by second-order zone boundary phonons) appears at 2692 cm^{-2} (Fig. 1b). The X-ray diffraction

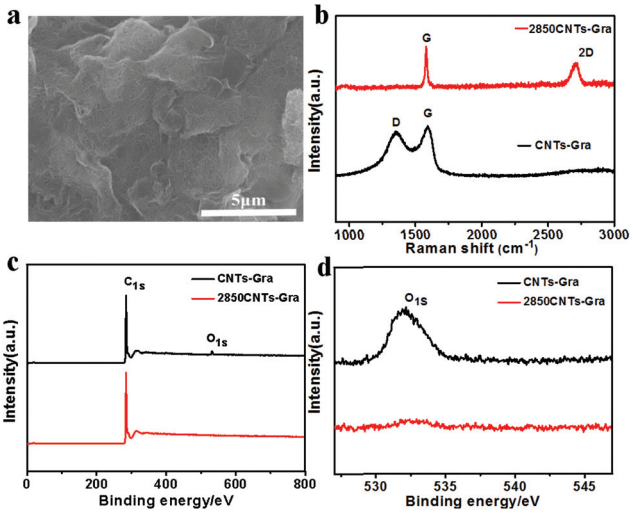

Fig. 1 (a) Typical SEM images of 2850CNTs–Gra; (b) Raman spectra and (c–d) XPS curves of the 2850CNTs–Gra and CNTs–Gra.

(XRD) pattern of 2850CNTs–Gra shows a much sharper and narrower peak at about $\theta = 26°$ compared with that of CNTs–Gra (Fig. S2b†). This demonstrates the ultrahigh graphite degree of 2850CNTs–Gra. X-ray photoelectron spectroscopy (XPS) analysis of 2850CNTs–Gra and CNTs–Gra was performed to determine the elemental composition. As shown in Fig. 1c and d, CNTs–Gra shows a dominant C 1s peak (284.8 eV) and a clear O 1s peak (532.0 eV). In contrast, there is only one C 1s peak in the spectrum of 2850CNTs–Gra. Nitrogen sorption isotherms (Fig. S3a†) and pore size distribution (Fig. S3b†) experiments show that the specific surface area (SSA) and specific pore volume (V_T) of 2850CNTs–Gra are 100.07 $m^2\ g^{-1}$ and 0.607 $cm^3\ g^{-1}$ (Table 1), respectively, which are much smaller than those of CNTs–Gra (SSA = 293.6 $m^2\ g^{-1}$ and V_T = 1.437 $cm^3\ g^{-1}$). It is speculated that this corresponds to the reduction of the oxygen content and SSA by ultrahigh temperature treatment because of the de-oxygenation and repair of the mesoporous structure by recombination of C–C bonds. Analogous results were obtained for single CNTs and graphene before and after ultrahigh temperature treatment (Table 1, Fig. S4a–f and S5a–f†). Adsorption experiments were also per-

Table 1 Textural properties of various samples

Sample	SSA[a] ($m^2\ g^{-1}$)	V_T[b] ($cm^3\ g^{-1}$)	V_{meso}[c] ($cm^3\ g^{-1}$)	V_{micro}[d] ($cm^3\ g^{-1}$)	Average pore[e] width per nm
2850Gra	68.35	0.314	0.298	0.016	18.25
Raw Gra	391.43	1.688	1.660	0.028	13.57
2850CNTs	119.04	0.866	0.853	0.013	24.12
Raw CNTs	227.93	1.375	1.353	0.022	21.76
2850CNTs–Gra	100.07	0.607	0.595	0.012	21.58
CNTs–Gra	293.64	1.437	1.419	0.018	15.18

[a] Specific surface area. [b] Total pore volume. [c] Mesopore volume. [d] Micropore volume. [e] Average pore size (estimated from the equation of 4VT/SBET).

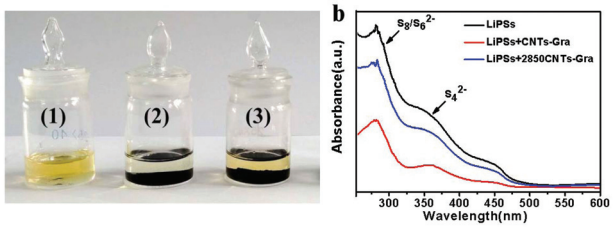

Fig. 2 Polysulfide permeation measurements. (a) Typical colors of solution from LiPSs (1), LiPSs/CNT–Gra (2) and LiPSs/2850CNTs–Gra (3) after 6 h; (b) the UV-vis absorption spectra of CNTs–Gra and 2850CNTs–Gra after soaking in the solution of LiPSs for 6 h.

formed to evaluate the PS trapping abilities of 2850CNTs–Gra and CNTs–Gra. As shown in Fig. 2a and b, 2850CNTs–Gra shows a poorer adsorption ability than CNTs–Gra. Combining with the XPS and adsorption experiment results, this may be due to the lower polar oxygenic functional group content and SSA of the 2850CNTs–Gra sample.

The electrochemical properties were evaluated by assembling standard 2025 coin cells (see the Experimental section). In the cyclic voltammetry (CV) curves of the 2850CNTs–Gra–S cathode (Fig. 3a), there are two cathodic peaks at 2.27 and 2.02 V, corresponding to the transition from the S_8 ring to long-chain PSs (Li_2S_x, $4 < x < 8$) and subsequent reduction to Li_2S_2 and Li_2S, respectively. The two anodic peaks at 2.38 and 2.42 V are ascribed to the conversion of LiPSs to active sulfur.[25,30] The second cycles of the CV plots for the two cathodes were investigated at a slow scan rate of 0.1 mV s^{-1} (Fig. 3b). There is a slightly positive shift in the 2850CNTs–Gra–S cathode reduction peak compared with that of CNTs–Gra–S, indicating that the 2850CNTs–Gra–S cathode possesses a lower potential polarization than the CNTs–Gra–S cathode.[27] Furthermore, the

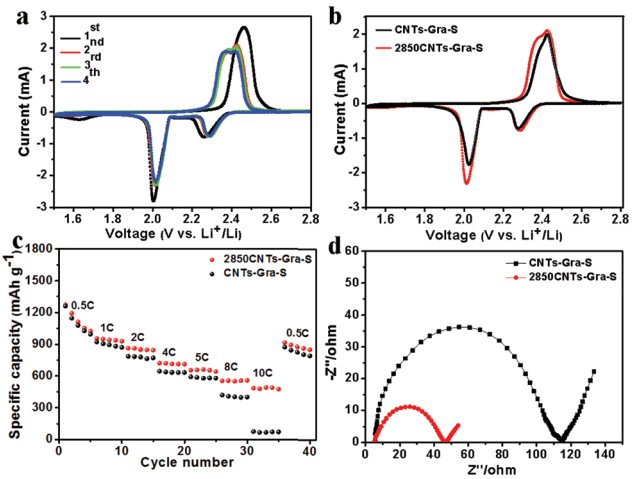

Fig. 3 (a) The first four cycles of cyclic voltammetry curves of the 2850CNTs–Gra cathode; (b) the second cyclic voltammetry curves of the 2850CNTs–Gra and CNTs–Gra cathode; (c) rate performance of the two cathodes at various current densities; (d) Nyquist plots of the two cathodes.

2850CNTs–Gra–S cathode has a higher collection coefficient (the ratio of the peak areas associated with the formation of Li_2S at ~2.0 V to that of the formation of LiPSs at ~2.4 V) (2.705) than the CNTs–Gra–S cathode (2.467). Considering its relatively poor adsorption ability compared with CNTs–Gra (Fig. 2a–b), it is speculated that 2850CNTs–Gra–S possesses much higher efficiency for the reaction between LiPSs and Li_2S_2/Li_2S than CNTs–Gra–S.

The rate performances of the two cathodes are shown in Fig. 3c and the charge–discharge profiles of the 2850CNTs–Gra–S cathode at various current rates are shown in Fig. S6c.† For current rates of 0.5, 1, 2, 4, 5, 8, and 10C, the 2850CNTs–Gra–S cathode delivers discharge capacities of 1023, 930, 843, 711, 660, 577, and 475 mA h g^{-1}, respectively. Additionally, a discharge capacity of 852 mA h g^{-1} can still be achieved when the current rate is abruptly changed from 10C to the initial current rate of 0.5C, suggesting that the cathode has excellent rate performance and good reversible capacity. For the raw CNTs–Gra–S cathode, lower discharge capacities (994 to 72 mA h g^{-1} for current rates of 1 to 10C) are observed under the same conditions. Electrochemical impedance spectroscopy (Fig. 3d) also shows that the 2850CNTs–Gra–S cathode has a lower charge-transfer resistance value than the raw CNTs–Gra–S cathode.

The difference values of the discharge capacity (D value, Fig. 4a) and the galvanostatic charge–discharge profiles of the 2850CNTs–Gra–S and CNTs–Gra–S cathodes were compared for current rates from 0.5 to 10C. At every rate, the 2850CNTs–Gra–S cathode shows better battery performances than the CNTs–Gra–S cathode, such as discharge capacity and polarization (Fig. 4b). After more detailed comparison, the improvement of the discharge capacity and polarization of the 2850CNTs–Gra–S cathode is more significant at faster cell operation (Fig. 4b–h). For example, at a current rate of 10C, the discharge capacity of the CNTs–Gra–S cathode is only 72 mA h g^{-1}, while a high discharge capacity of 475 mA h g^{-1} is maintained for 2850CNTs–Gra–S. All of these observations verify that 2850CNTs–Gra exhibits good promise as a host material, in reducing the potential polarization and increasing the discharge capacity, especially at high current rates.

Cycling stability is an important property of Li–S batteries. Owing to the advantages of the 2850CNTs–Gra–S cathode at high current rates, the long-term cycling stability was investigated at the current rates of 10C and 15C (Fig. 5a–b and Fig. S7†). As shown in Fig. 5a, compared with the CNTs–Gra–S cathode, the 2850CNTs–Gra–S cathode has a higher discharge capacity, from an initial capacity of 627 to 306 mA h g^{-1} over 1000 charge–discharge cycles at 10C with a decay rate of 0.051% per cycle. Remarkably, the 2850CNTs–Gra–S cathode exhibits excellent cycling stability at a high current rate of 15C (Fig. 5b). The initial discharge capacity of the 2850CNTs–Gra–S cathode is 158 mA h g^{-1} and it gradually increases to 314 mA h g^{-1}. This can be ascribed to the electrochemical activation process of sulfur particles. In this process, sulfur particles transform into active PSs and then dissolve in the electrolyte. After the initial activation, the cell reaches maximum sulfur

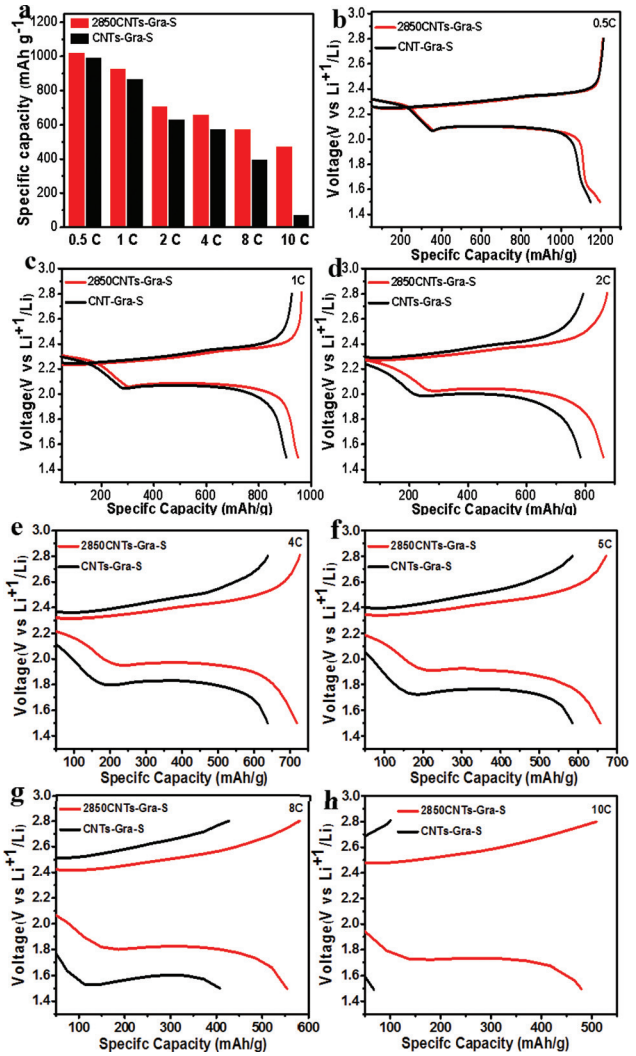

Fig. 4 (a) Discharge capacity and (b–h) galvanostatic charge/discharge profiles of the 2850CNTs–Gra–S and CNTs–Gra–S cathodes at 0.5, 1, 2, 4, 5, 8 and 10C rates.

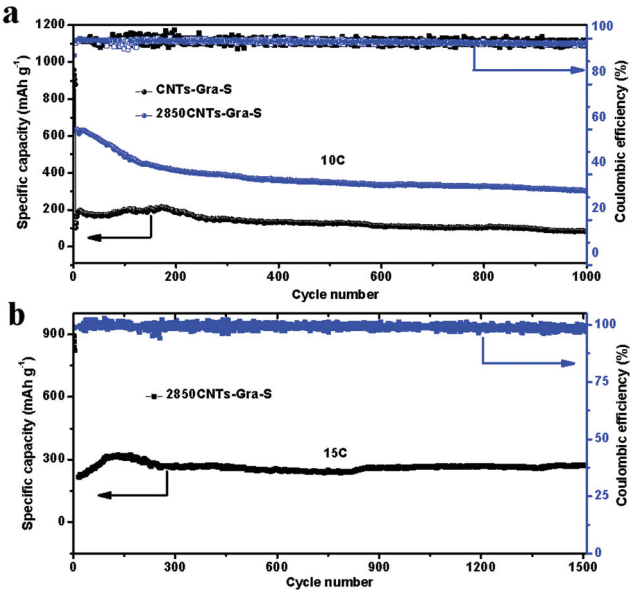

Fig. 5 (a) Cycling performance of CNTs–Gra–S and 2850CNTs–Gra–S cathode at the rate of 10C; (b) prolonged cycling performance of the 2850CNTs–Gra–S cathode at the rate of 15C.

utilization and then maintains a stable coulombic efficiency of about 99% in subsequent cycles. After 1500 charge–discharge cycles at 15C, the 2850CNTs–Gra–S cathode retains a capacity of 273 mA h g^{-1}, and the decay rate is 0.0087% based on the maximal discharge capacity of 314 mA h g^{-1}. Such a low decay rate of 0.0087% at 15C has rarely been reported.

A cathode with an areal sulfur loading >3 mg cm^{-2} is necessary for the practical application of Li–S batteries in hybrid electric vehicle (HEV) and electric vehicle (EV) batteries.[31] Thus, a 2850CNTs–Gra–S cathode with a sulfur loading of 3.03 mg cm^{-2} was fabricated by increasing the electrode thickness. The 2850CNTs–Gra–S cathode with 3.03 mg cm^{-2} sulfur mass loading exhibits an initial capacity of 1201 mA h g^{-1} at a current rate of 0.1C (0.507 mA cm^{-2}) (Fig. S8†) After 350 cycles at 1C (5.075 mA cm^{-2}), the discharge capacity is 440 mA h g^{-1} with the capacity retention of about 80% (based on the maximum discharge capacity of 550 mA h g^{-1}) and the coulombic efficiency of 97%, while the CNTs–Gra–S cathode with the same sulfur loading does not work at a current rate of 1C.

To investigate why the 2850CNTs–Gra–S cathode possesses long-term and stable cycling performance at high current rates, comparative experiments of the 2850CNTs–S, 2850Gra–S, and 2850CNTs–Gra–S cathodes were performed (Fig. S9†). The rate performance of 2850CNTs–Gra–S is better than those of 2850CNTs–S and 2850Gra–S, further demonstrating the advantage of the 3D network structure of 2850CNTs–Gra. Additionally, comparing the cycling performance results for raw CNTs–S, 2850CNTs–S, raw Gra–S, and 2850Gra–S (Fig. S10a and b†), ultrahigh temperature treatment is beneficial for greatly improving the cycling performance.

The separator is an essential part of the battery configuration and it plays a crucial role in preventing internal short circuits and maintaining the diffusion path for ions.[32] For 2850CNTs–Gra–S and CNTs–Gra–S, we disassembled the four cycled cells at rates of 1, 2, 8, and 10C inside a glovebox. SEM images of the obtained separators are shown in Fig. 6a–h. At low current rates (1 and 2C), there is no obvious damage of the separators (2850CNTs–Gra–S and CNTs–Gra–S). When the current rate is increased to 10C, the separator for CNTs–Gra–S shows widespread damage (Fig. 6d), while the separator for 2850CNTs–Gra–S is relatively integrated after operation under the same conditions (Fig. 6h). Considering the galvanostatic charge–discharge profiles and potential polarization for the two samples (Fig. 4h), we believe that the widespread damage of the separator for the CNTs–Gra–S cathode will cause the cell to seriously deteriorate at 10C. In this regard, protecting the integrity of the separator and revealing the corresponding protection mechanism at high current rates are important to ensure stable operation of the cell. Therefore, we further dis-

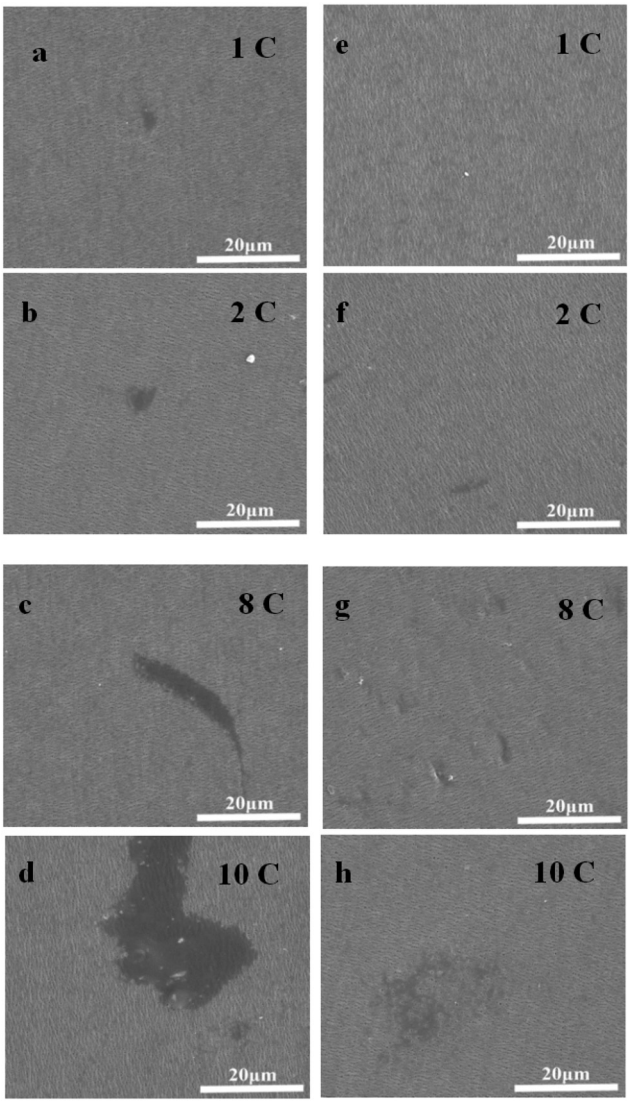

Fig. 6 The SEM images of separators collected from CNTs–Gra–S (a–d) and 2850CNTs–Gra–S (e–h) at 1C, 2C, 8C and 10C after working under the same conditions.

assembled a series of cycled cells corresponding to the four cathodes (CNTs–Gra, 2250CNTs–Gra, 2550CNTs–Gra and 2850CNTs–Gra). From the SEM images of these cycled cathodes at a current density of 10C as shown in Fig. S11,† the 2850CNTs–Gra showed that the discharge products were uniformly deposited and distributed, while the other three cathodes appeared porous with agglomerated discharge products. Considering the properties of the nearly ideal sp^2 hybridized carbon network of the host material (*e.g.*, high electrical and thermal conductivity),[29] it is speculated that protection of the separator and improvement of the rate performance by 2850CNTs–Gra can be attributed to two factors: (1) the promoted transformation from solid Li_2S_2/Li_2S to soluble LiPSs,[33–37] which has been proven by CV and tests of the cell performance (Fig. 3–5), can guarantee uniform deposition and distribution of solid products, leading to reduction in the volume expansion of the electrode. (2) The high thermal conductivity of the sp^2 hybridized carbon network can achieve efficient heat dissipation of the joule heating at a high current rate during cell operation to maintain the integrity of the separator.

Conclusion

We have coupled a sp^2 carbon configuration consisting of 3D carbon nanotubes/graphene prepared by ultrahigh temperature treatment (2850 °C) with S for application in Li–S batteries. The 2850CNTs–Gra–S cathode delivers a considerable specific capacity after 1500 cycles and exhibits an extremely low capacity degradation rate of 0.0087% per cycle working at a current rate of 15C. The excellent performance of 2850CNTs–Gra is ascribed to the properties of sp^2 carbon materials, such as the 3D network structure, outstanding conductivity, efficient heat dissipation, and intriguing functionality to protect the separator integrity. It is believed that this strategy of ultrahigh temperature treatment to form an ideal sp^2 hybridized structure can not only be used to prepare host materials for sulfur in Li–S batteries, but can also be applied to other energy storage systems.

Experimental section

Synthesis of CNTs–Gra and 2850CNTs–Gra

The raw carbon nanotubes and graphene were purchased from a commercial corporation. The CNTs and graphene (2 : 1 by mass) were ultrasonically dispersed in an alcoholic solution for 120 minutes, and then the mixture was dried in an oven at 80 °C. The obtained material was called CNTs–Gra. The CNTs–Gra was further heated to 2850 °C under ambient Ar for 2 hours in an ultrahigh temperature graphitized furnace. The obtained material was called 2850CNTs–Gra. As the control experiment, the other materials were obtained under various conditions, such as the temperature, the mass ratio of CNTs and graphene and time. They were named 2250CNTs–Gra, 2550CNTs–Gra, 2850^1CNTs–Gra and so on.

Synthesis of 2850CNTs–Gra–S

The 2850CNTs–Gra–S composites were prepared following a melt-diffusion strategy. Specifically, the 2850CNTs–Gra and sulfur (high purity sulfur, 99.99% metal basis, Aladdin) were mixed. And then the powder was ground and heated in an oven at 160 °C for 12 h, followed by another 12 h at 180 °C. From ESI Fig. S6a and b,† the sulfur was uniformly distributed in the 2850CNTs–Gra. The sulfur contents in this work were determined to be 65.5 wt%. For comparison, the other composites were prepared *via* the same method.

Structure characterization

X-ray photoelectron spectroscopy (XPS) measurements were carried out with an ultrahigh vacuum setup, equipped with a

monochromatic Al KR X-ray source and a high resolution Gammadata-Scienta SES 2002 analyzer. X-ray diffraction patterns (XRD) were obtained with a D/MAX-2400 diffractometer using Cu Kα radiation (40 kV, 100 mA, λ = 1.54056 Å). Raman spectra were tested under ambient conditions using a Renishaw (inVia) with an Ar-ion laser beam at an excitation wavelength of 532 nm. The nitrogen adsorption/desorption data were recorded at the liquid nitrogen temperature (77 K) using a Micromeritics ASAP 2020 M apparatus. The samples were degassed at 200 °C under vacuum for 3 h prior to the measurement. The pore size distribution (PSD) was derived from the adsorption branch of the isotherms using the Barrett–Joyner–Halenda (BJH) model. The total pore volumes were calculated from the amount adsorbed at a relative pressure (P/P_0) of 0.99. The specific surface area was calculated using the Brunauer–Emmett–Teller (BET) equation. SEM images were obtained with a JSM-6700F field-emission scanning electron microscope. TEM analyses were carried out with a JEOL-3010 instrument operating at 200 kV. The samples for TEM analysis were prepared by adding dehydrated alcohol droplets of the products on copper grids and drying at 45 °C. Thermogravimetric analysis (TGA) was carried out at a heating rate of 10 °C min^{-1} under a nitrogen flow, using a STA449 F3 Jupiter thermogravimetric analyzer (NETZSCH).

Electrochemical characterization

In our experiments, for any sample, we have prepared and tested six cells under the same working conditions. Electrochemical experiments were performed *via* CR2025 coin-type test cells assembled in an argon-filled glovebox with lithium metal as the counter and reference electrodes at room temperature. The cathode for the Li–S batteries was fabricated *via* mixing 90 wt% composite materials, 5 wt% conductive agent and 5 wt% polyvinylidene difluoride (PVDF) in *N*-methyl-2-pyrrolidone (NMP) to form a slurry. Subsequently, the slurry was pasted onto an aluminum foil and dried at 60 °C overnight. A Celgard 2400 membrane was used as the separator to isolate electrons. The electrolyte was 1 M bis(trifluoromethane)sulfonimide lithium salt (LiTFSI) with 1% $LiNO_3$ dissolved in a mixture of 1,3-dioxolane (DOL) and dimethoxymethane (DME) (1 : 1 by volume). The amount of electrolyte is 50 μL in a coin cell for the areal sulfur loading of 0.8 mg cm^{-2} and when the areal sulfur loading is increased to 3.03 mg cm^{-2}, the corresponding amount of the electrolyte is increased to 250 μL, respectively. Cyclic voltammetry (CV) and electrochemical impedance spectroscopy (EIS) measurements were performed on a CHI6600 electrochemical workstation. The scan rate of CV measurements was set to be 0.1 mV s^{-1}, and the DC voltage was kept at open-circuit voltage and an AC voltage of 5 mV in amplitude was applied with a frequency of 200 kHz to 20 mHz in EIS measurements.

Conflicts of interest

There are no conflicts to declare.

Acknowledgements

The work was supported in part by grants from the National Natural Science Foundation of China (51741207, 51572197, 21475096, 51420105002), the Natural Science Foundation of Zhejiang Province for Distinguished Young Scholars (LR18E020001), the Science and Technology Project of Zhejiang Province (LGF18B050005) and the State Key Laboratory of Structural Chemistry (20170035).

References

1 J. Q. Huang, T. Z. Zhuang, Q. Zhang, H. J. Peng, C. M. Chen and F. Wei, Permselective Graphene Oxide Membrane for Highly Stable and Anti-self-discharge Lithium-sulfur Batteries, *ACS Nano*, 2015, **9**, 3002–3011.
2 M. Wild, L. O'Neill, T. Zhang, R. Purkayastha, G. Minton, M. Marinescu and G. J. Offer, Lithium Sulfur Batteries, a Mechanistic Review, *Energy Environ. Sci.*, 2015, **8**, 3477–3494.
3 P. G. Bruce, S. A. Freunberger, L. J. Hardwick and J. M. Tarascon, Li-O_2 and Li-S Batteries with High Energy Storage, *Nat. Mater.*, 2012, **11**, 19–29.
4 Y. Yang, G. Zheng and Y. Cui, ChemInform Abstract: Nanostructured Sulfur Cathodes, *Chem. Soc. Rev.*, 2013, **42**, 3018–3032.
5 A. Manthiram, Y. Fu and Y. S. Su, Challenges and Prospects of Lithium-sulfur Batteries, *Acc. Chem. Res.*, 2013, **46**, 1125–1134.
6 Q. Pang, D. Kundu, M. Cuisinier and L. F. Nazar, Surface-Enhanced Redox Chemistry of Polysulphides on a Metallic and Polar Host for Lithium-sulphur Batteries, *Nat. Commun.*, 2014, **5**, 4759.
7 J. Zhang, H. Hu, Z. Li and X. W. Lou, Double-Shelled Nanocages with Cobalt Hydroxide Inner Shell and Layered Double Hydroxides Outer Shell as High-Efficiency Polysulfide Mediator for Lithium-Sulfur Batteries, *Angew. Chem., Int. Ed.*, 2016, **55**, 3982–3986.
8 Q. Zhang, Y. Wang, W. S. Zhi, Z. Fu, R. Zhang and Y. Cui, Understanding the Anchoring Effect of Two-Dimensional Layered Materials for Lithium–Sulfur Batteries, *Nano Lett.*, 2015, **15**, 3780.
9 X. Tao, Y. Liu, W. Liu, G. Zhou, J. Zhao, D. Lin, C. Zu, O. Sheng, W. Zhang and H. Lee, Solid-State Lithium-Sulfur Batteries Operated at 37 °C with Composites of Nanostructured $Li_7La_3Zr_2O_{12}$/Carbon Foam and Polymer, *Nano Lett.*, 2017, **17**, 2967–2972.
10 M. Q. Zhao, X. F. Liu, Q. Zhang, G. L. Tian, J. Q. Huang, W. Zhu and F. Wei, Graphene/Single-Walled Carbon Nanotube Hybrids: One-Step Catalytic Growth and Applications for High-Rate Li–S Batteries, *ACS Nano*, 2012, **6**, 10759–10769.
11 H. Hu, H. Cheng, Z. Liu, G. Li, Q. Zhu and Y. Yu, In Situ Polymerized PAN-Assisted S/C Nanosphere with Enhanced High-Power Performance as Cathode for Lithium/Sulfur Batteries, *Nano Lett.*, 2015, **15**, 5116–5123.

12 J. Zhang, C. P. Yang, Y. X. Yin, L. J. Wan and Y. G. Guo, Sulfur Encapsulated in Graphitic Carbon Nanocages for High-Rate and Long-Cycle Lithium–Sulfur Batteries, *Adv. Mater.*, 2016, **28**, 9539–9544.

13 Z. Ma, L. Tao, D. Liu, Z. Li, Y. Zhang, Z. Liu, H. Liu, R. Chen, J. Huo and S. Wang, Ultrafine Nano-Sulfur Particles Anchored on in Situ Exfoliated Graphene for Lithium–Sulfur Batteries, *J. Mater. Chem. A*, 2017, **5**, 9412–9417.

14 C. Tang, B. Li, Q. Zhang, L. Zhu, H. Wang, J. Shi and F. Wei, CaO-Templated Growth of Hierarchical Porous Graphene for High-Power Lithium–Sulfur Battery Applications, *Adv. Funct. Mater.*, 2016, **26**, 577–585.

15 D. Rao, Y. Wang, L. Zhang, S. Yao, X. Qian, X. Xi, K. Xiao, K. Deng, X. Shen and R. Lu, Mechanism of Polysulfide Immobilization on Defective Graphene Sheets with N-Substitution, *Carbon*, 2016, **110**, 207–214.

16 G. Li, J. Sun, W. Hou, S. Jiang, H. Yong and J. Geng, Three-Dimensional Porous Carbon Composites Containing High Sulfur Nanoparticle Content for High-Performance Lithium-Sulfur Batteries, *Nat. Commun.*, 2016, **7**, 10601.

17 S. Liu, X. Xia, Y. Zhong, S. Deng, Z. Yao, L. Zhang, X. Cheng, X. Wang, Q. Zhang and J. Tu, 3D TiC/C Core/Shell Nanowire Skeleton for Dendrite-Free and Long-Life Lithium Metal Anode, *Adv. Energy Mater.*, 2018, **8**, 1702322.

18 H. J. Peng, J. Q. Huang, M. Q. Zhao, Q. Zhang, X. B. Cheng, X. Y. Liu, W. Z. Qian and F. Wei, Carbon: Nanoarchitectured Graphene/CNT@Porous Carbon with Extraordinary Electrical Conductivity and Interconnected Micro/Mesopores for Lithium-Sulfur Batteries, *Adv. Funct. Mater.*, 2014, **24**, 2920–2920.

19 X. Han, Y. Xu, X. Chen, Y. C. Chen, N. Weadock, J. Wan, H. Zhu, Y. Liu, H. Li and G. Rubloff, Reactivation of Dissolved Polysulfides in Li–S Batteries Based on Atomic Layer Deposition of Al_2O_3 in Nanoporous Carbon Cloth, *Nano Energy*, 2013, **2**, 1197–1206.

20 X. Tao, J. Wang, C. Liu, H. Wang, H. Yao, G. Zheng, S. Z. Wei, Q. Cai, W. Li and G. Zhou, Balancing Surface Adsorption and Diffusion of Lithium-Polysulfides on Nonconductive Oxides for Lithium–Lulfur Battery Design, *Nat. Commun.*, 2016, **7**, 11203.

21 H. J. Peng, G. Zhang, X. Chen, Z. W. Zhang, W. T. Xu, J. Q. Huang and Q. Zhang, Enhanced Electrochemical Kinetics on Conductive Polar Mediators for Lithium-Sulfur Batteries, *Angew. Chem., Int. Ed.*, 2016, **55**, 13184–13189.

22 T. Lei, W. Chen, J. Huang, C. Yan, H. Sun, C. Wang, W. Zhang, Y. Li and J. Xiong, Multi-Functional Layered WS_2 Nanosheets for Enhancing the Performance of Lithium-Sulfur Batteries, *Adv. Energy Mater.*, 2017, **7**, 1601843.

23 Z. Sun, J. Zhang, L. Yin, G. Hu, R. Fang, H. M. Cheng and F. Li, Conductive Porous Vanadium Nitride/Graphene Composite as Chemical Anchor of Polysulfides for Lithium-Sulfur Batteries, *Nat. Commun.*, 2017, **8**, 14627.

24 Z. Xiao, Z. Yang, L. Zhang, H. Pan and R. Wang, Sandwich-Type NbS2@S@I-Doped Graphene for High-Sulfur-Loaded, Ultrahigh-Rate, and Long-Life Lithium-Sulfur Batteries, *ACS Nano*, 2017, **11**, 8488–8498.

25 L. Wang, Z. Yang, H. Nie, C. Gu, W. Hua, X. Xu, X. a. Chen, Y. Chen and S. Huang, A Lightweight Multifunctional Interlayer of Sulfur-Nitrogen Dual-Doped Graphene for Ultrafast, Long-Life Lithium-Sulfur Batteries, *J. Mater. Chem. A*, 2016, **4**, 15343–15352.

26 Z. Xiao, Z. Yang, L. Wang, H. Nie, M. Zhong, Q. Lai, X. Xu, L. Zhang and S. Huang, A Lightweight TiO_2/Graphene Interlayer, Applied as a Highly Effective Polysulfide Absorbent for Fast, Long-Life Lithium-Sulfur Batteries, *Adv. Mater.*, 2015, **27**, 2891–2898.

27 W. Hua, Z. Yang, H. Nie, Z. Li, J. Yang, Z. Guo, C. Ruan, X. Chen and S. Huang, Polysulfide-Scission Reagents for the Suppression of the Shuttle Effect in Lithium-Sulfur Batteries, *ACS Nano*, 2017, **11**, 2209–2218.

28 L. Peng, Z. Xu, Z. Liu, Y. Guo, P. Li and C. Gao, Ultrahigh Thermal Conductive yet Superflexible Graphene Films, *Adv. Mater.*, 2017, **29**, 170589–170597.

29 C. Teng, D. Xie, J. Wang, Z. Yang, G. Ren and Y. Zhu, Ultrahigh Conductive Graphene Paper Based on Ball-Milling Exfoliated Graphene, *Adv. Funct. Mater.*, 2017, **27**, 1700240–1700247.

30 H. A. Salem, G. Babu, C. V. Rao and L. M. R. Arava, Electrocatalytic Polysulfide Traps for Controlling Redox Shuttle Process of Li–S Batteries, *J. Am. Chem. Soc.*, 2015, **137**, 11542–11545.

31 D. Lv, J. Zheng, Q. Li, X. Xie, S. Ferrara, Z. Nie, L. B. Mehdi, N. D. Browning, J. G. Zhang and G. L. Graff, High Energy Density Lithium–Sulfur Batteries: Challenges of Thick Sulfur Cathodes, *Adv. Energy Mater.*, 2015, **5**, 1402290.

32 J. Q. Huang, Q. Zhang and F. Wei, Multi-Functional Separator/Interlayer System for High-Stable Lithium-Sulfur Batteries: Progress and Prospects, *Energy Storage Mater.*, 2015, **1**, 127–145.

33 S. E. Cheon, K. S. Ko, J. H. Cho, S. W. Kim, E. Y. Chin and H. T. Kim, Rechargeable Lithium Sulfur Battery I. Structural Change of Sulfur Cathode During Discharge and Charge, *J. Electrochem. Soc.*, 2003, **150**, A796–A799.

34 S. E. Cheon, S. S. Choi, J. S. Han, Y. S. Choi, B. H. Jung and S. L. Hong, Capacity Fading Mechanisms on Cycling a High-Capacity Secondary Sulfur Cathode, *J. Electrochem. Soc.*, 2004, **151**, A2067–A2073.

35 Q. Pang, J. Tang, H. Huang, X. Liang, C. Hart, K. C. Tam and L. F. Nazar, A Nitrogen and Sulfur Dual-Doped Carbon Derived from Polyrhodanine@Cellulose for Advanced Lithium–Sulfur Batteries, *Adv. Mater.*, 2015, **27**, 6021–6028.

36 K. Han, J. Shen, S. Hao, H. Ye, C. Wolverton, M. C. Kung and H. H. Kung, Free-Standing Nitrogen-Noped Graphene Paper as Electrodes for High-Performance Lithium/Dissolved Polysulfide Batteries, *ChemSusChem*, 2014, **7**, 2545–2553.

37 W. Luo, L. Zhou, K. Fu, Z. Yang, J. Wan, M. Manno, Y. Yao, H. Zhu, B. Yang and L. Hu, A Thermally Conductive Separator for Stable Li Metal Anodes, *Nano Lett.*, 2015, **15**, 6149–6154.